High-Speed 2D-Digital Image Correlation to Quantify Energy Mitigation Behaviors of Engineered Elastomeric Materials Subjected to Shock

Undergraduate Honors Thesis

Presented in Partial Fulfillment of the Requirements for Graduation with Distinction in the Department of Mechanical and Aerospace Engineering of The Ohio State University

By

Peter Vuyk

Honors Undergraduate Program in Mechanical Engineering

The Ohio State University

December 2018

Thesis Committee:

Ryan L. Harne, Advisor

Ruike Zhao

ABSTRACT

Engineered, elastomeric material damping systems have revealed striking ability to attenuate shock loads at the macroscopic level. Reports suggest that this capability is associated with the reversible elastic buckling of internal beam constituents observed in quasistatic characterizations. Yet, the presence of buckling members induces non-affine response at the microscale, so that clear understanding of the exact energy dissipation mechanisms remains clouded. In this report, we examine a mechanical metamaterial that exhibits both micro- and macroscopic responses under impact loads and devise an experimental method to visualize the resulting energy dissipation mechanisms using 2D Digital Image Correlation (DIC). Without existing standards for applying 2D-DIC for studying high strain rates of absorbent, viscoelastic material structures, a novel approach for executing 2D-DIC visualization was implemented using charcoal powder. Simultaneously collected force transmission data and DIC analysis associated with the deformation of test specimens under impact loading reveal a bridge for studying the microscale interactions that culminate in macroscale deformation. To illustrate the potential of this application, this experiment was carried out on specimens with varying, but known, quasistatic loading behaviors to verify and validate discrepancies between quasi-static and dynamic loading. This process illuminates the influence of dynamic strain distribution throughout the material's in-plane cross-section on its overall tendency to buckle uni- or bimodally, thus dissipating injected force with varying degrees of force transmission and pulse duration. With this understanding, we uncover a strategy for geometrically programing the macroscopic deformation to enhance impact mitigation properties.

ACKNOWLEDGEMENTS

I would first like to thank my advisor and mentor Dr. Harne, for his persistent and unwavering support of me and my research endeavors, as well as his patience in motivating me to achieve success when I did not at first believe that I could.

I also want to thank Dr. Ruike Zhao for her contributions and expertise as my defense committee member.

Additionally, I would like to thank all members of the Laboratory of Sound and Vibration Research (LSVR) team for their helpfulness and patience in assisting me throughout my undergraduate research.

This work is supported in part by Owens Corning Science and Technology and in part by the Haythornthwaite Foundation. All related experiments in this research are conducted at LSVR, directed by Dr. Harne.

TABLE OF CONTENTS

LIST OF FIGURES

LIST OF TABLES

1 INTRODUCTION

1.1 Background on shock absorption of buckling structures

The motivation to study shock absorption for the protection of people, systems, and sensitive components has long demanded the application of state-of-the-art scientific rigor for mitigating high amplitude impulse force transmission. An effective and proven solution to this problem of shock mitigation is the application of buckling beam lattices for shock absorption [1] [2] [3] [4] [5]. Applications where this class of solution is pertinent spans from electronic packaging and commercial building sub-flooring to football helmets [6] and car bumpers [7]. In the latter pair of examples, large amplitude force injections occur occasionally, but must be capable of mitigating substantial shock injections when collision occurs, given the fact that these material systems are protecting people. Additionally, the application of elastomeric beam-based structures has long been an area of significant development [1] [8] [9] [10] [11], due lightweight, reusable, and viscoelastic characteristics inherent to this class of materials. Elastomers composed of silicone-rubber material are synthetically manufactured and affordable for small batch production, encouraging its usage for studying recoverable shock absorption solutions. Despite recent advances in the application of multi-stable and viscoelastic materials for shock absorption, a visual technique for studying the local interactions of these engineered systems is still out of reach. Given recent advances in the application of digital image correlation (DIC) [12] [13] for studying deforming materials [14] in a non-invasive manner, this technique is suitable for studying the dynamic response to impact with the desired visualized feedback of this research.

1.2 Research goal

The goal of this research is to implement 2D Digital Image Correlation (DIC), along with established methods of modal hammer data force data collection, in order to reveal and validate unique dynamic force transmission characteristics associated with variations in variable elastomer beam thickness configurations. By aligning captured frames with corresponding input and output force measurements in time, the relationship between instantaneous motion and strain of deforming specimens and the force pulse characteristics that precipitate this dynamic behavior, can be visualized and studied. With an effective approach for correlating force with specimen motion, the effect of internal beam thickness variations on force transmissibility and output force pulse time duration can be validated in terms of instantaneous, local buckling behavior.

1.3 Thesis overview

The content of this thesis is organized in the following manner. Chapter 2 describes the methods for setting up and executing the experimental procedure followed to collect time-aligned captured images and corresponding force input and output data. This chapter also discusses the application of DIC to generate strain and displacement contours for studying the influence of buckling behavior on force transmission properties. Chapter 3 summarizes the gathered results and discusses the influence of beam geometry variations on buckling behavior and buckling behavior on force transmission. Finally, Chapter 4 presents the conclusions from this research and answers the aforementioned purpose.

2 EXPERIMENTAL METHODS

In order to quantify the unique force transmission characteristics associated with variable beam thickness, simultaneous high-speed image capture, input modal hammer force, and output force transducer data are collected for three unique elastomer geometric configurations. The following chapter will describe the specimen undergoing experimental study, as well as the process of preparing it for DIC analysis. Subsequently, the separate impact hammer and high-speed image capture setups are described. Finally, the process of aligning the images and force data with one another in time, as well as the methodology of executing DIC analysis, are addressed.

2.1 Specimen design and fabrication

The elastomer material used to fabricate the specimens to be tested is Mold Star™ 15S. A pre-cured mixture of this silicone rubber is poured into a 3D-printed negative of the desired specimen. Once the specimen has cured completely, the 3D-printed parts can be de-molded, and the elastomer specimen extracted. All three specimens studied contain eleven vertical beams in each layer between three horizontal beams that compose the length of the specimen. A solid control specimen is also fabricated and tested to provide a baseline for force transmission properties of the geometries under study. The three fabricated specimens are hereafter referred to as Uniform, R-class, and L-class. Figure 1 contrasts the geometric attributes that make the three specimens unique.

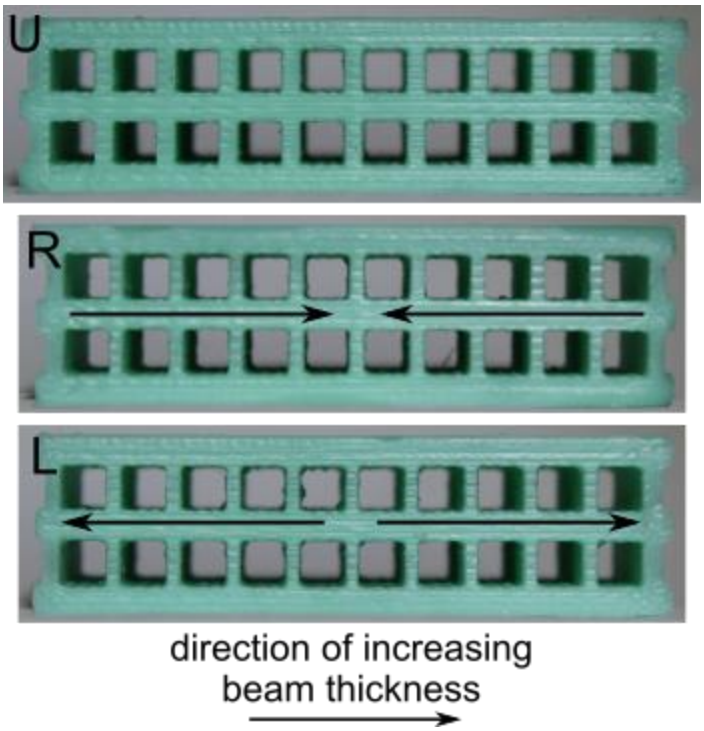

Figure 1: Shown are, from top to bottom, the Uniform, R-class, and L-class specimen. The uniform geometry contains beams of equal thickness. The R-class geometry contains beams whose thickness scales linearly from the outermost beams to the innermost beam. The L-class geometry contains beams whose thickness scale linearly from the innermost beam to the outermost beams.

2.2 Specimen preparation for 2D-DIC

In order to apply DIC analysis to these fabricated elastomeric specimens, a novel approach for creating conventional image correlation speckled patterns on viscoelastic, polymer-based material surfaces required development. Due to the absorbent nature of these materials, a non-liquid based technique was employed. By applying diffusely charcoal-speckled patterns to the surface that will undergo DIC analysis, this method for minimally-invasive study can be utilized without modifying the sensitive mechanical properties of these soft material architectures. An overview of the speckling process described is illustrated in Figure 2.

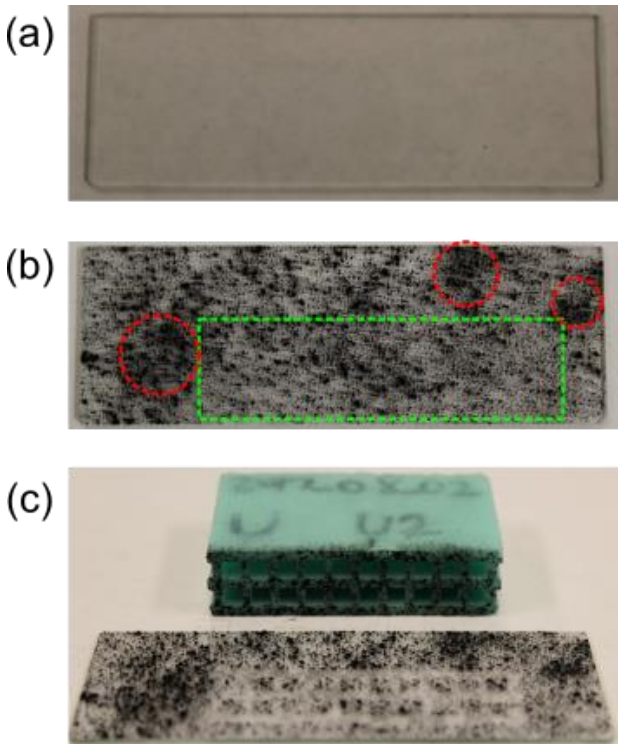

Figure 2: Process overview for 2D-DIC preparation of elastomer specimens. (a) Start with a clean glass slide; (b) Create a diffuse speckle pattern on the slide avoiding over-speckled areas identified by red circles. The area enclosed by a green rectangle identifies an area the size of the application face containing adequate speckling; (c) A speckled specimen after application.

In order to apply the charcoal speckling pattern to the specimen, a clean glass slide is first prepared and placed on a white background to provide clarity when preparing the pattern. Next, the speckled pattern is created on the glass slide using a toothpick. To do this, the toothpick was inserted into a container of activated charcoal powder so that a layer of powder collects on its surface, and is subsequently spun rapidly between the thumb and middle finger to create a diffuse expulsion about 6" above the surface of the glass slide. This motion of the thumb and middle finger closely resembles the act of snapping ones finger and is critical for ensuring a diffuse accumulation of charcoal powder on the slide. A diffusely speckled pattern with equal areas of charcoal powder and empty glass slide is ultimately desired, yet manual application will limit a perfect execution of this. A diffuse pattern that does not contain large areas of either empty glass slide or charcoal

clumping will be sufficient for performing DIC analysis. Continue to repeat the process of applying charcoal to the slide until an area slightly larger than the surface of the specimen contains a completed speckle pattern.

Next, gently press the surface containing the beam architecture of interest against the area of the slide containing the pattern to be applied. In doing this, ensure that the surface normal of the application face is parallel to that of the glass slide, and that the specimen is pressed against the slide with only enough force to adhere the charcoal to the surface of the specimen. This will mitigate stretching and sliding of the application face across the charcoal-covered slide, a maneuver that can cause smearing that is detrimental to DIC results. Mishaps that lead to uneven, smeared, or clumped speckle patterns are washed off under cold water, and the specimen is subsequently pat dried and allowed time to completely air dry before re-attempting his process. The end result of the speckling process applied to the three unique geometries of interest is shown in Figure 3.

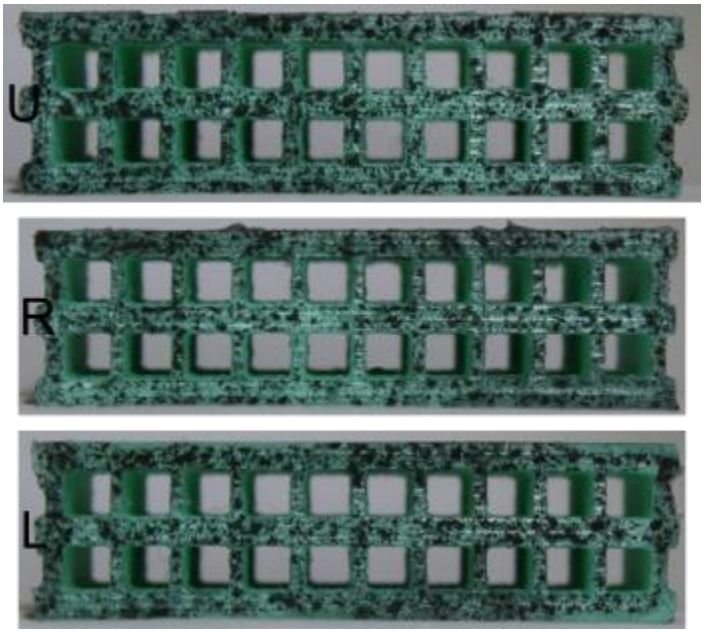

Figure 3: Final speckled Uniform, R-class, and L-class specimens.

2.3 Experimental setup

The physical setup is composed of two distinct elements: the modal hammer and force transducer for gathering data related to force transmission and the high-speed camera and lighting apparatus for obtaining images of the deforming specimen. Each setup is distinct but must also consider the needs of the other for ensuring that the data can be represented cohesively during post-processing.

2.3.1 Impact hammer setup

The modal hammer experiments require that the specimen be minimally constrained between two rigid surfaces. The rigid constraint is provided by two 1/8” aluminum 6063 constraining plates. The bottom plate is longer than the top plate in order to allow space for a guitar tuner (YMC Chrome Tuning Peg Round 220-3L3R) to be fixed to the end. Fishing wire (Tebco Omniflex 50 lb 0.029 dia) is fed through holes in the corner

of the top plate, through corresponding holes in the bottom plate, and, finally, through the guitar tuner. A knot is tied at the end of each constraining wire to prevent it from slipping through the top plate. The adjustment of the fishing wire with the guitar tuner therefore manipulates the degree of pre-constraint applied to specimen prior to impact. To make room for the tuner peg sticking out beneath the bottom plate, five 1/4"-20 fender washers are mounted on a 3/4" length of #10-32 threaded rod used to connect the bottom plate to the output force transducer. Another segment of #10-32 threaded rod is used to fix the force transducer to a machined aluminum mounting block beneath the transducer. The aluminum block is fastened to isolation table, upon which all experimentation takes place, using two 1/4"-20 bolts. This setup can be seen in Figure 4.

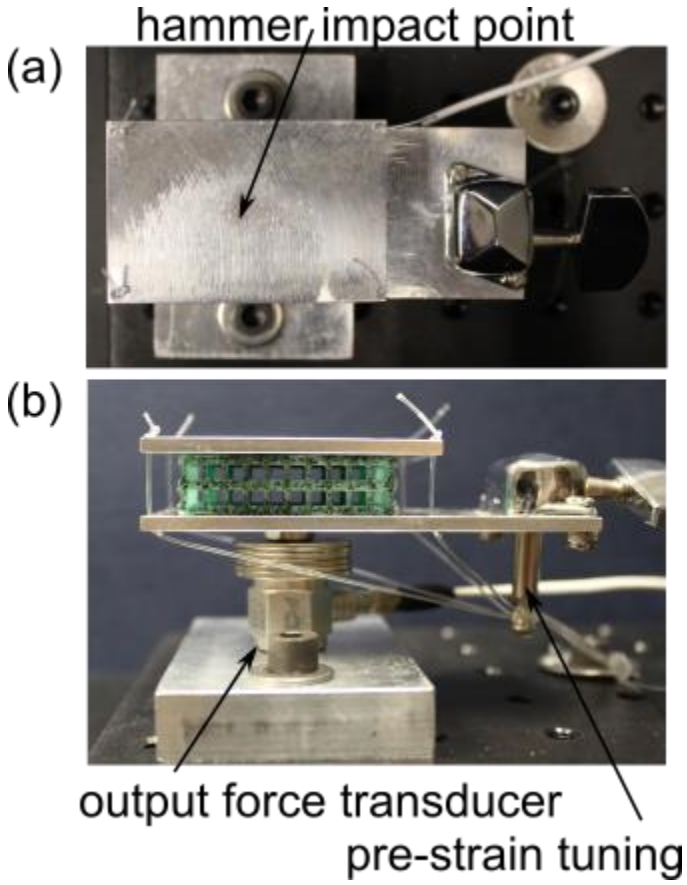

Figure 4: Constraining plate and tuner assembly used to adjust the initial constraint applied to a specimen prior to impact. (a) Top view of constraining plate assembly showing centralized orientation of hammer impact; (b) Front facing view of a speckled uniform specimen constrained between a top and bottom plate that is mounted to the output force transducer.

When fastening the components of this assembly to one another and the table, great care is taken to ensure that, ultimately, the surface of the specimen to be mounted between the aluminum plates is facing outward to where the high-speed camera will be setup for imaging.

The modal hammer (PCB 086C03) is used to inject a known force amplitude into the top surface of the specimen via the rigid aluminum plate, and the time series output force amplitude is collected with the output force transducer (PCB 208C03) attached to the bottom plate. Both signals are fed through a signal conditioner (PCB 8162011A) and into a data acquisition system (NI USB 6341 Multifunction DAQ). The voltage

readings are sampled at 131072 Hz to avoid aliasing during impact data collection. Prior to testing, the specimen is lightly constrained to prevent translation of the specimen upon impact, without initiating buckling of the vertical beams. Since the specimens are fabricated with an initial basic specimen height parallel to the direction of input force of 12 mm, the pre-constraint applied to achieve the aforementioned effect is within 0.02 mm of 11.8 mm for all four constraining corners. The level of constraint is measured using digital dial calipers (iGaging OrignCal) to ensure that the specimen is being uniformly constrained between the plates.

Two sets of trials are completed for each specimen. The first set consists of 100 evenly distributed hits between 50 N and 700 N for each of the four specimens, including the solid control. For each set of 100 hits, the input and output force time series are assessed to determine the peak input and output force, as well as the output pulse time duration.

The second trial set consists of three hits with simultaneous corresponding high-speed image capture, for each of the beam-composed trials. The three hits are hereafter termed as Hit 1, 2, and 3, and refer to varying magnitudes of peak input force. Hit 1 is a light hit of approximately 150 N which is not sufficient to incite contact of the horizontal beams with one another, termed compaction. Hit 2 is a medium hit of approximately 300 N which is the approximate threshold of force required to cause compaction of the specimen. Finally, Hit 3 is a hard hit of approximately 500 N which will cause compaction for all three specimens.

2.3.2 High-speed camera setup

In order to accompany the three hit trials with image capture for DIC analysis, a high-speed camera (Photron FastCam SA-X2) with a light source (Nitecore Concept 1 flashlight) must be setup facing the speckled elastomer face. The camera is mounted on a Manfrotto tripod to allow for adjusting of the height. The flashlight is similarly mounted with a microphone stand so that the light can be focused on the specimen during imaging. Because the frame rate of image capture is 50,000 fps, the light source is used on its highest setting to provide adequate illumination, despite the reduction of light passing through the lens that accompanies high shutter speeds. A lens with large aperture (Nikon AF-S DX NIKKOR 35mm f/1.8G) is used with the high-speed camera. The setup is shown in Figure 5.

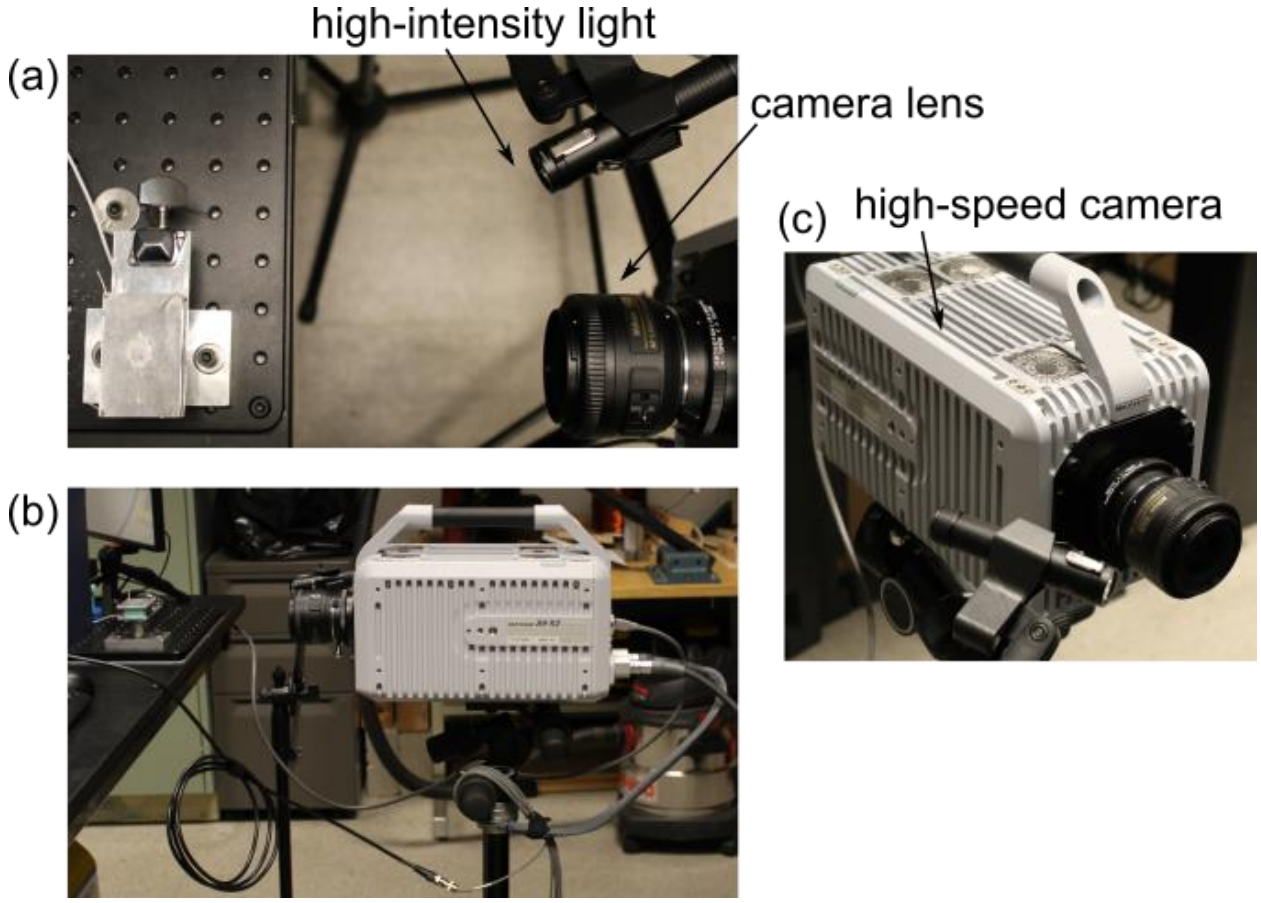

Figure 5: High-speed camera setup in front of modal hammer assembly. (a) Top view of camera and light source directed at deforming, speckled elastomer face; (b) Side view of camera assembly with the power cable going off-screen to the right, the Ethernet cord plugging into the camera above the power cable, and the trigger signal connecting to a BNC that leads to the signal conditioner; (c) Front view of the camera with an adjustable lens and a flashlight mounted in a microphone stand.

Once setup, the camera is connected to a 120 VAC wall outlet power source using the stock power cable. Images are transferred to a computer for DIC analysis via an Ethernet connection. Finally, in order to ensure that image capture and force data collection can be time-aligned for video playback, a +5 V TTL trigger pulse of approximately 1 microsecond is sent to the signal conditioner when image capture is triggered.

2.4 Time-alignment of transducer and image capture data

After the modal hammer and high-speed camera setup have been assembled, the Photron FastCam Viewer 3 (PFV) software is used to set a hardware image trigger that sends a trigger pulse when image capture initiates. A MATLAB incoming data listener object is created to handle the incoming TTL trigger data from the camera, and initiates force data collection when the +5 V signal is received. A data/image buffer is implemented in MATLAB and PFV to allow for saving of data/images captured prior to the trigger event. The strategy of a data buffer is employed to ensure that force data and image capture for the entirety of an impact event are encompassed in the collected and saved data. Subsequently, using the known trigger frame and event time, as well as the data and image capture rates, video playback containing time series force data and corresponding DIC can be synchronized in time.

A trigger event in PFV is set to occur when the levels of luminosity for a user-defined area exceed a user-specified quantity. By using an angled, dark background, the area above the top aluminum plate is assured to always be very near to zero, because little light is reflected back to the lens from the background. Therefore, the trigger region can be defined as an area just above the top plate with height of approximately 20 mm and width of 12 mm. The user-specified luminosity threshold for initiating a trigger event can be set conservatively because the baseline luminosity is already near-zero with the dark, angled background. For the three hit trials, this threshold value was set to ±5 lumens about the baseline value of 5 lumens. Therefore, when a luminosity of 10 lumens was reached, the camera would send a TTL pulse and begin image capture. When the reflective, metallic surface of the hammer enters this trigger region preceding an impact event, the luminosity averages over 80 lumens, implying that a threshold of 10 lumens is more than sufficient for ensuring consistent triggering immediately before impact. Besides the benefit of time-aligned force timer series data and captured image playback, utilizing a trigger to initiate data collection ensures consistency in that for every hit registered by the camera hardware, there will be an outputted TTL pulse which incites corresponding force data collection.

2.5 Applying 2D-DIC to captured frames

Once the total set of captured frames for each specimen and hit have been trimmed to contain only the frames with meaningful corresponding force data, the images are ready to be prepared for DIC analysis. Using IrfanView 64, an open source graphic viewer that allows for batch image editing, these frames are cropped to contain only the specimen. Both trimming frame count and cropping frame content increases the computational efficiency of running DIC on a large quantity of high resolution images.

Next, DIC analysis is performed utilizing MATLAB-based 2D-DIC code originally presented as part of a challenge paper submission by Dr. Elizabeth Jones. The only modifications made to the Jones DIC script are related to formatting and description of output figures as well as the bypassing of the included GUI. Otherwise, all functionality is described in her publication and associated documentation.

The first step in the process of optimizing DIC parameters, is determining an appropriate subset size that corresponds to a correlation coefficient. Subset size corresponds to the level of discretization that all frames in a set of frames experience for groups of speckles. In other words, it is the side length, in pixels, of the square encompassing the area on the specimen that is tracked through the impact event. Since the specimen itself is small and takes up a small proportion of the captured frame, the speckles that are used to create surface contrast, are relatively small (in terms of pixel count per speckle) compared to many traditional DIC applications. For this reason, a subset size of 11 pixels is used for generating the tracking function. The next critical DIC parameter to set is the step size. The step size determines the number of data points that will be tracked to produce the final DIC visual. Since each data point represents a grayscale average of a subset, the step size determines the number of subsets that are averaged in each frame to compute data points that are correlated to corresponding data points in the previous frame. For higher resolution DIC results, a smaller step size is desired. In the case of this research, a step size of 2 was used due, in large part, to the already minimal number of total pixels that compose the specimen in a frame. In general, a small subset size will reduce the number of pixels averaged per data point and a small step size will decrease the pixels between

each data point for a user-defined grid. The grid, in this case, is defined as the area over the un-deformed specimen, or the first frame in a correlated set of frames. Once the DIC parameters have been optimized to produce a clear and sensible result for the severest displacement case (Hit 3), the procedure is applied to all image sets serially, using the first image in a set as the reference image, or the frame to be correlated against for each subsequent frame in a set. The DIC parameters used to produce the displacement contours for each impact event are summarized in Table 1.

Table 1: DIC parameters optimized for generating displacement contours from captured frames.

Parameter	Value
Subset Size (px)	11
Step Size (px)	2
Computation Method	Serial
Reference Frame	First

Once the displacement contours have been generated, the void spaces are removed by manually removed data points corresponding to areas in the reference frame that do not correspond to a speckled surface. Next, the strain component contours are computed and the strain and displacement contours are smoothed using linear interpolation between data points. Finally, the deformed grid that deforms with the specimen is created by applying the displacements at each point in each frame, to the reference grid.

3 RESULTS AND DISCUSSION

From the experimentally obtained data, baseline dynamic characteristics associated with impact events are defined in order to identify deviations from this baseline associated with variable beam thickness scaling. Comparing the dynamic behavior with known quasistatic responses associated with variable beam thickness scaling, similarities in the dynamic and quasistatic behavior are validated. In order to uncover trends related to deviation from expected behavior, the high-speed captured image frames with corresponding DIC strain and displacement contours are turned to.

3.1 Impact force transmission characteristics

Force input and output data collected for each specimen present certain common attributes that can be used to develop a baseline for comparing the force transmission characteristics of fabricated variable beam thickness specimens. As shown for the Uniform specimen in Figure 6, the input and output force are hereafter shown as blue and red lines, respectively. The input force imparted by the modal hammer, intuitively, peaks first, initiating the impact event. Following this initial peak of injected force, the output put force peaks as a result of the initial peak input force. For a given hit, the output force pulse duration is the time it takes for the initial increase in output force to reduce back to zero. Longer pulse durations are desirable in many engineering applications of shock mitigation due to the reduction in momentum increase explained by the impulse momentum theorem.

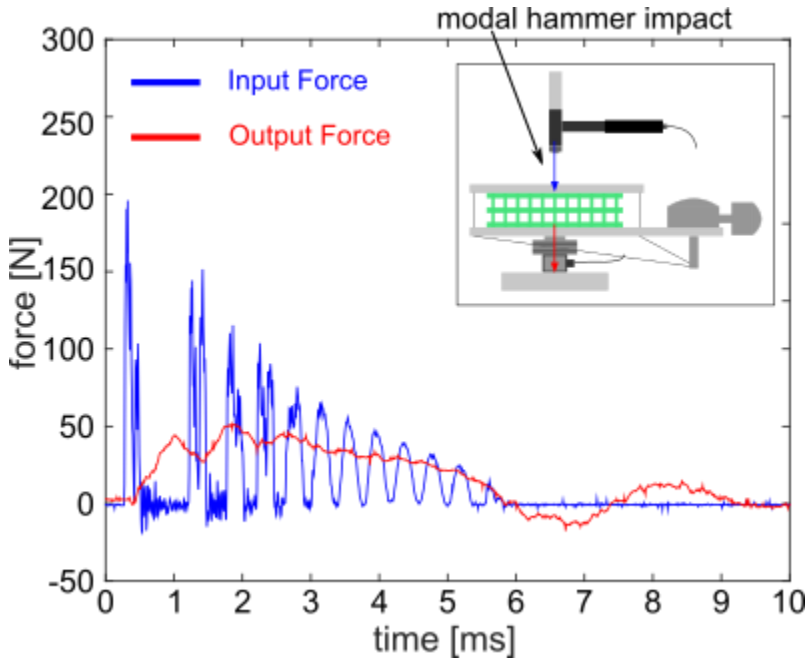

Figure 6: Force input and output for low amplitude impact of the Uniform specimen. Force input by the modal hammer is given in blue and the force experienced by the force transducer is given in red.

Given this basic understanding of the relationship between input and output impact force through these solid structures, a more rigorous study of the dependence of output force and output force pulse duration on input force can be undertaken. The 100 hit trials of varying of input force for each specimen provide insight into

the relationship between these key force transmission properties and the injected force from the modal hammer. By summarizing the peak input and output forces, as well as output pulse duration, this connection is evident. As seen in Figure 7, there exists clear bilinear trend in output force versus input force. Further study shows that the critical input force that precedes the second linear regime is the force required to completely buckle a specimen and cause compaction. Prior to this compaction point, the beams are pre-buckled and buckling. The output force pulse duration correspondingly shows this pre-buckled and buckling critical input force with clarity. The output force pulse duration is constant prior to buckling, due to the direct transmission of force through the vertical, un-buckled beams, resulting in pure compression. In the regime where the beams are buckling, an increase in pulse duration trend arises. The span of input forces resulting in increasing output fore pulse duration can be attributed to the degrees of buckling that the vertical beams can experience for given input forces. At a second critical input force, the degree of buckling provides diminishing increases in pulse duration so that the pulse duration begins to decrease with increasing input force. This regime is termed post-buckling. Post-buckling occurs prior to compaction, as is seen when comparing the critical point input forces in Figure 7.

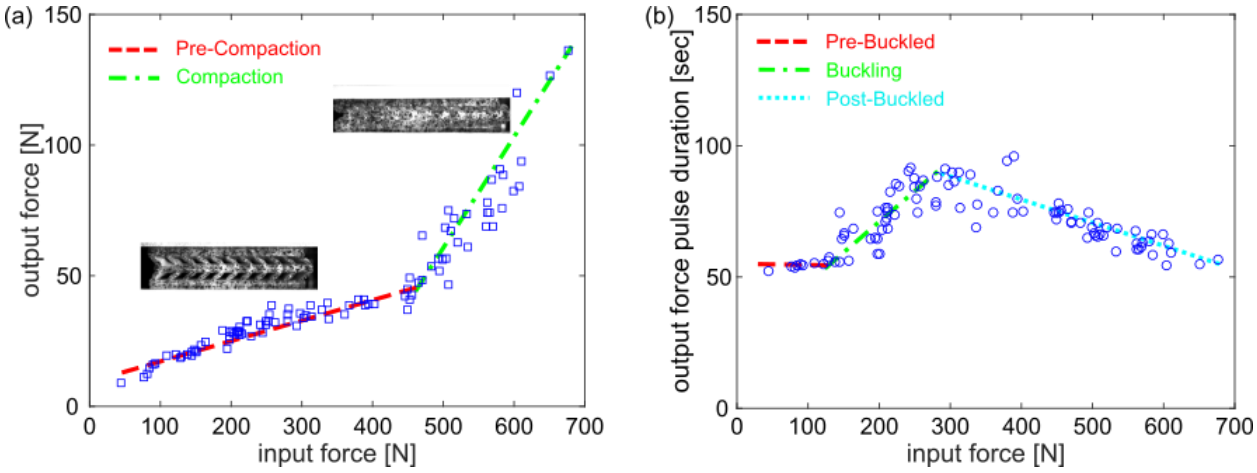

Figure 7: (a) Input force versus output force showing two distinct regimes: pre-compaction encompasses buckled and pre-buckled behavior and compaction occurs after the injected force causes the horizontal beams to contact one another; (b) The output force pulse duration shows three regimes corresponding to beam response to input force: pre-, during, and post-buckled states.

Be explicitly defining the force transmission characteristics of this class of impacted specimens, the variable characteristics in response for varying beam thickness, a tailorable parameter, can be evaluated relative to baseline behavior.

3.2 Influence of geometric variations on buckling behavior

By linearly scaling the gradient of beam thickness laterally along the parallel vector to the horizontal beams, the buckling properties, and thus, force transmission properties of this class of material structures can be manipulated. In the case of this research, the applied beam thickness gradient contains it thickest and thinnest beams on its inner and outer most beams so that the structure is symmetric about it innermost beam. This simple reversal in beam gradient changes the segment of the structure most likely to buckle first. The first

beam to buckle influences the direction of buckling of the adjacent beams, thus encouraging collective beam buckling behavior. Figure 8 shows FEA results for an ABAQUS Implicit analysis that illustrates the influences on strain contours when the position of the least stable beam is altered under quasistatic displacement.

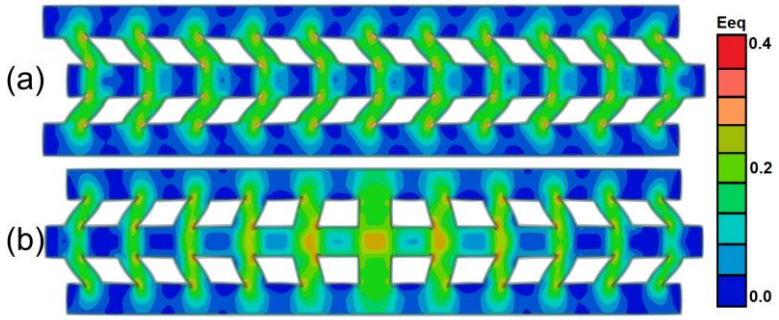

Figure 8: FEA model for finite equivalent plane strain (E_{eq}) illustrating the difference in specimen buckling behavior; (a) uniform specimen buckling unimodal and collectively; (b) r-class specimen buckling bimodal consists of opposing collective buckling responses that originate around an inner beam.

The model results in Figure 8 are from previous work in Vuyk et. al. [14]. The FE study assumes plane strain conditions which neglects the influence of any out-of-plane deformation. The material properties used for the Neo-Hookean solid hyperelastic material model are provided in Table 2. The Láme parameters listed are derived from the empirically-determined Young's Modulus of Elasticity and density, as well as an assumed Poisson's ratio that is consistent with prior knowledge of elastomers. A fixed boundary condition is applied to the bottom surface and the displacement was applied to the top surface. Additionally, horizontal displacement of the top beam was inhibited. Finally, a quadrilateral mesh was implemented with adequate density to produce consistent plane strain contours.

Table 2: List of material properties for generating the FE results of the uniform and r-class specimens in Figure 8.

Young's modulus of elasticity, E [kPa]	752
density, ρ [kg/m^3]	1,145
Poisson's ratio, ν [dim]	0.49
Láme's first parameter, λ [MPa]	12.36
Láme's second parameter, μ [kPa]	252.3

The model assumed a quasi-static applied displacement that is uniform, yet the results elegantly introduce the two modes of buckling seen in this class of engineered structures: unimodal and bimodal buckling. Unimodal buckling results when a single mode dominates the collective lateral motion of buckling about the center horizontal beam. Bimodal buckling results when an interior beam shows a significantly varying potential to buckle when compared to its adjacent counterparts. In a quasi-static application such as the FE model, this

potential difference arises as a result of significant beam thickness gradient from center to outer beams. A thicker beam requires a greater applied load to buckle than a thinner variant of that same beam. Therefore, the beams will buckle about the inner node of buckling potential difference, leading to opposing lateral motion, termed bimodal buckling.

3.3 Influence of buckling behavior on force transmission

With an understanding of how buckling behavior can be tailored with variable beam thickness gradient, the influence of buckling behavior on the measurable force transmission characteristics discussed in Section 3.1, can be assessed. Figure 9 shows the 100 hit peak output force and pulse duration plotted versus input force for the three beam architectures and a solid control. Notably, the control specimen shows a linear trend for both transmission properties having the highest force transmission lowest pulse duration for all input forces.

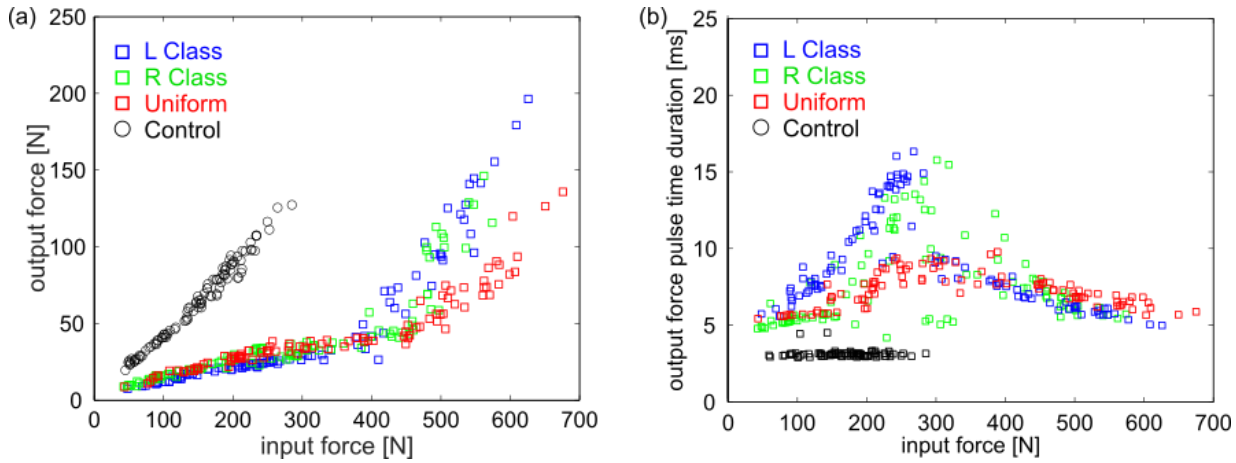

Figure 9: 100 hit trials for three beam-composed structures and a solid control comparing the differences in force transmission properties for different beam geometry variations. (a) Output force versus input force; (b) Output force pulse duration versus input force.

It is evident that the compaction region shows a slope of peak output versus input force that is similar to the solid control specimen, suggesting that during compaction, the specimens begin to behave like solid elastomers with force transmission properties matching that of the control. For lower input forces, the force transmission is less for the L-class specimen that it is for the R-class and uniform specimen. Yet, the L-class specimen exhibits higher force transmission than the other two specimens for forces great enough to induce compaction. This seems to suggest a trade-off in force transmission that is largely dependent on the level input force.

On the other hand, L- and R-class specimens demonstrate a greater increase in pulse duration than the uniform during buckling, which suggests that input forces great enough to cause buckling to occur but small enough to precede the occurrence of compaction, are more sensitive to beam thickness variations than those forces not within this range. Since buckling behavior is known to be influenced by beam thickness gradients present in the L- and R-class specimens for quasi-static displacement, it is reasonable to question whether or not the dynamic buckling characteristics are also influenced by these gradients. The output force pulse duration for varying input forces further begs this question.

In order to explain the trends assessed in the 100 hit trials, DIC is applied to frames captured for three hit levels for each specimen. The output force time series for each specimen plotted with the same hit number as the other two beam-composed specimens is shown in Figure 10.

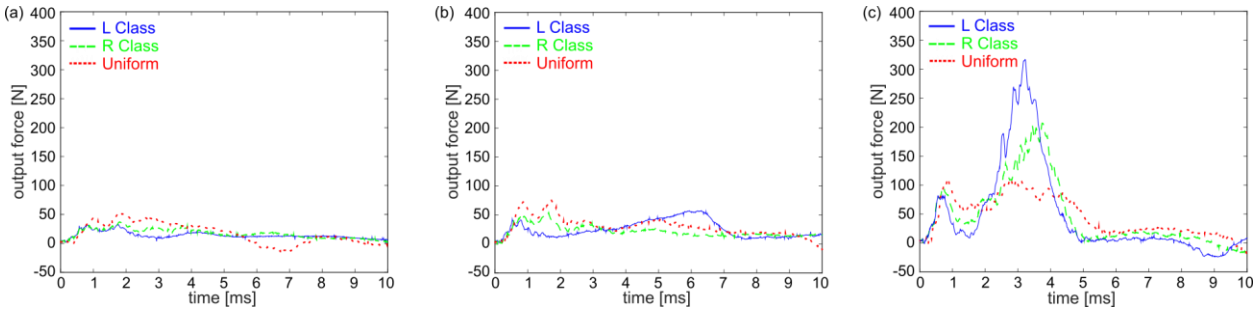

Figure 10: Output force time series for specimens of varying linear beam scaling. (a) Hit 1 – Low input force that incites buckling; (b) Hit 2 – Medium input force post-buckling and near compaction; (c) Hit 3 – High input force that causes horizontal beam compaction.

From the output force pulse duration plots, emphasizing the fact that each plot is for the same peak input force amplitude, the trends noticed in the 100 hit trials can be validated. The Uniform and R-class specimens shows similar trends in peak output force, following very similar trace with uniform having slightly higher output force amplitude for low input forces (Figure 10a and 10b). For the higher input forces, the R- and L- class specimens have similarly increased output force peaks and pulse durations, while the Uniform specimen does not show this larger peak. This suggests that perhaps compaction did not occur for the Uniform specimen, as the 100 hit trials show all specimens behave like the solid control, with nearly 50% force transmission, when compaction has occurred. The DIC results in the following section validate this and prior trends noticed throughout this chapter.

3.4 Characterizing dynamic force trends with DIC analysis

Applying DIC to three critical input forces provides a visual element that can be leveraged for studying the dissipation mechanisms that lead to unique force transmission characteristics. The following section will individually verify trends in the DIC results that validate force transmission data for each specimen.

The force data corresponding to the uniform hits are summarized in Figure 11. The uniform specimen exhibits a relatively flat pulse duration across all input forces, reaching a peak of ~10 ms during a buckled response to injected force.

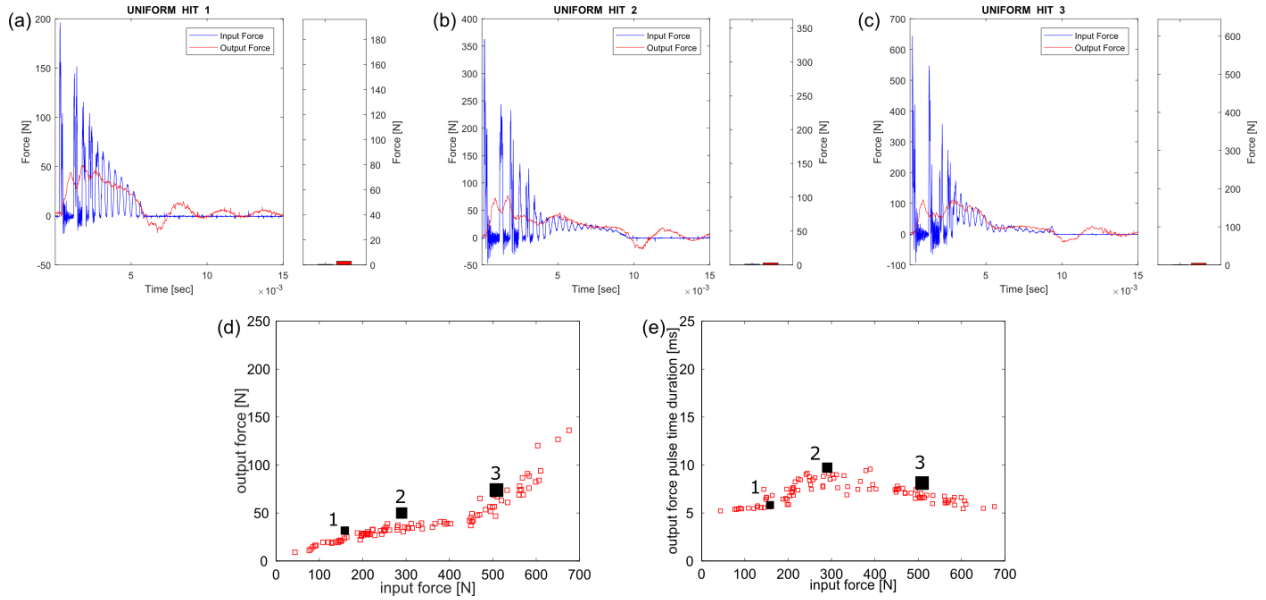

Figure 11: Input and output force time results for each hit of the Uniform specimen with corresponding image capture. (a) Hit 1 input versus output force time series (b) Hit 2 input versus output force time series; (c) Hit 3 input versus output force time series; (d) Hit 1-3 position on 100 hit trial results for output versus input force; (e) Hit 1-3 position on 100 hit trial results for output force pulse duration.

The three hits, Hit 1-3, correspond to a pre-buckled, buckled, and nearly compacted event as illustrated by in Figure 12. In this and later figures, the finite plane strain and displacement magnitude components are labeled as identified in Table 3.

Table 3: Description of displacement and finite plane strain component notation in playback of frames with DIC analysis

Notation	Full Description
Disp	Displacement Magnitude
E_{xx}	X Normal
E_{yy}	Y Normal
E_{xy}	Shear
E_{eq}	Equivalent

The last image in all DIC snapshot figures is the moment of peak displacement in the impact event. In the case of the uniform specimen, an initial bimodal response is apparent for all three input force amplitude regimes. In Section 3.2, the instigator for a bimodal response was defined as being a difference in the potential for two adjacent beams to buckle. In the FE example provided in Figure 8, this potential difference was a result of increased center beam thickness. However, for the uniform geometry, the beam thickness is uniform, so the potential difference due to beam thickness does not explain bimodal uniform response. Another source of adjacent beam buckling potential difference, is localized impact forces. Since the impact force is applied at a point centered over the vertical beam array, the first beam to buckle is directly beneath the impact force. If the initial force causes perfect compression of the center beam without lateral deflection, the beam will stiffen, causing the surrounding beams to deflect outward (Figure 12a1-a5). This resistance of the center beam to buckle causes the uniform specimen to have a higher force transmission at low input forces.

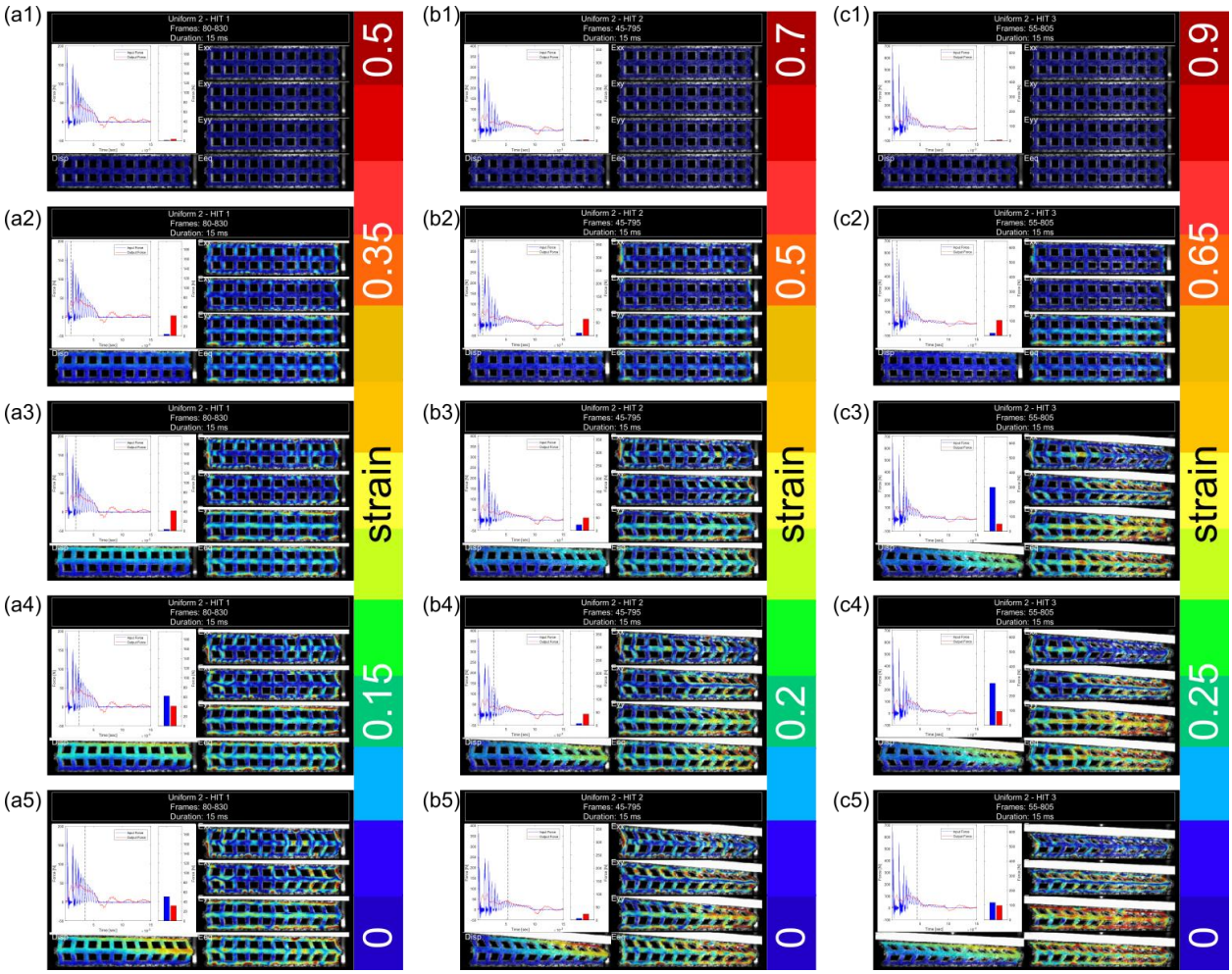

Figure 12: Snapshots highlighting full impact sequence for all three Uniform hits: (a) Hit 1, (b) Hit 2, and (c) Hit 3.

Another observation to note is that the uniform specimen does not achieve full compaction (Figure 12 c5) for the high amplitude input force hit. This is clear due to the presence of small void spaces between the buckled columns. Full compaction entails the complete compression of the horizontal beams into one another, causing the void spaces to be non-existent. This explains the lack of a steep output force peak that is attributed to compacted beams. A final critical takeaway from the DIC breakdown of the uniform hits is the ultimate transfer of the bimodal response to a collective uniform response for Hit 2 and 3 (Figure 12 b/c1-5). For high enough input forces, the left side is pulled laterally by the horizontal beam as seen for the lateral strain component labeled E_{xx}. The horizontal beam shows a patch of high lateral strain that originates at the beam buckling potential difference node and translates left until the last beam has shifted into collective behavior.

The force data corresponding to the L-class hits is presented in Figure 13. Similar to the uniform hits, each L-hit corresponds to a pre-buckled, buckled, and nearly compacted event. The L-class specimen exhibits low force transmission for Hits 1 and 2, but quickly behaves similarly to the solid control upon compaction, with a near 50% force transmission.

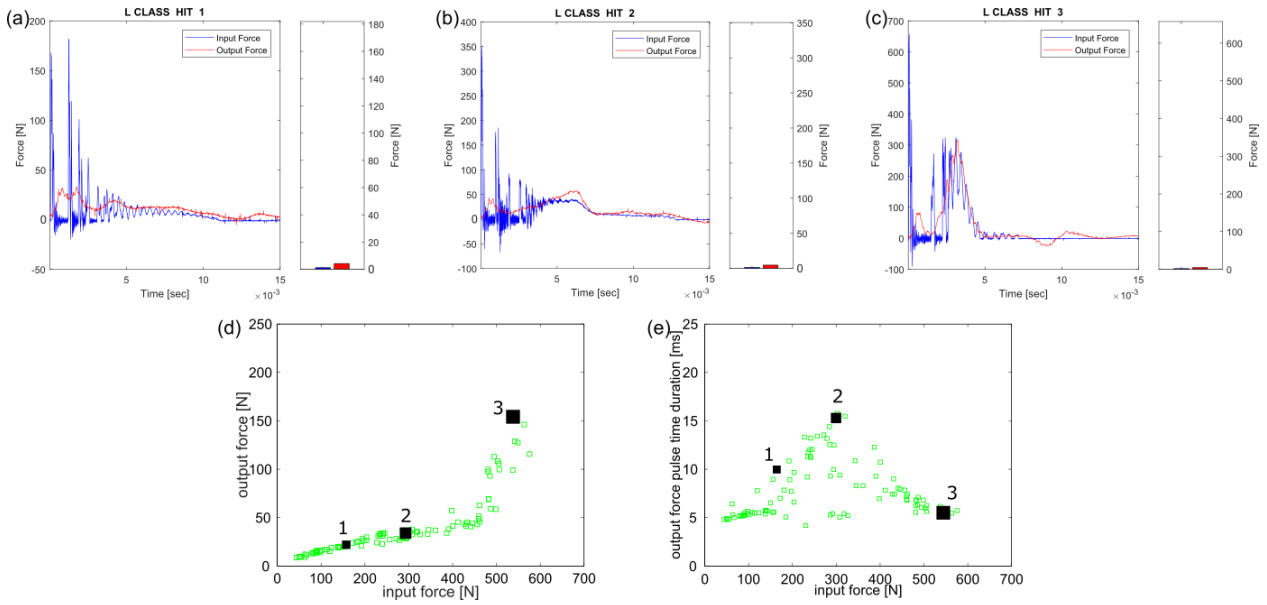

Figure 13: Input and output force time results for each hit of the L-class specimen with corresponding image capture. (a) Hit 1 input versus output force time series (b) Hit 2 input versus output force time series; (c) Hit 3 input versus output force time series; (d) Hit 1-3 position on 100 hit trial results for output versus input force; (e) Hit 1-3 position on 100 hit trial results for output force pulse duration.

Unlike the uniform hits, however, the L-class specimen buckles with collective unimodal behavior, regardless of input force, as is evident in all three hit sequences illustrated by Figure 14. For all input force amplitudes, the middle beam buckles first as a result of being the thinnest beam in the array (Figure 14 a/b2). This induces the unimodal buckling predicted by the quasi-static response. When the middle beam buckles, the surrounding beams buckle collectively with the subsequent lateral motion of the horizontal beam. This causes a complete mitigation of the lateral strain (E_{xx}) that arises in the horizontal beam for a bimodal response. In addition, it takes less force to achieve the increased pulse duration that accompanies buckling.

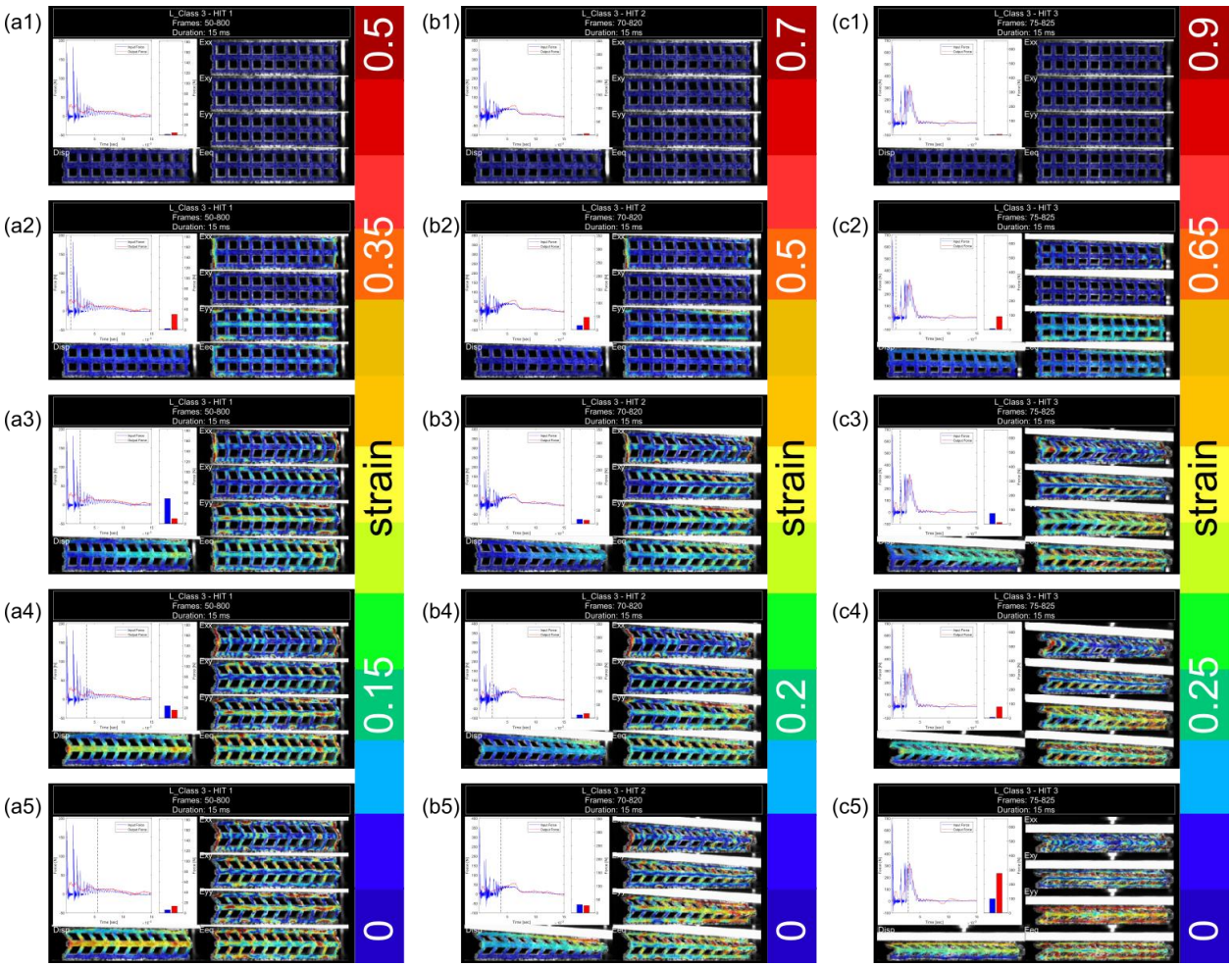

Figure 14: Snapshots highlighting full impact sequence for all three L-class hits: (a) Hit 1, (b) Hit 2, and (c) Hit 3.

The force data corresponding to the R-class hits is presented in Figure 13. The force time series for R-class Hits 1 and 2 closely resemble the Uniform time series in that they have a lower output force response for a given low amplitude force input. On the other hand, the pulse duration for the output force response is higher for Hit 1 than in the case of the Uniform Hit 1. Additionally, the output force amplitude for the high amplitude input force clearly indicates a compaction event has occurred.

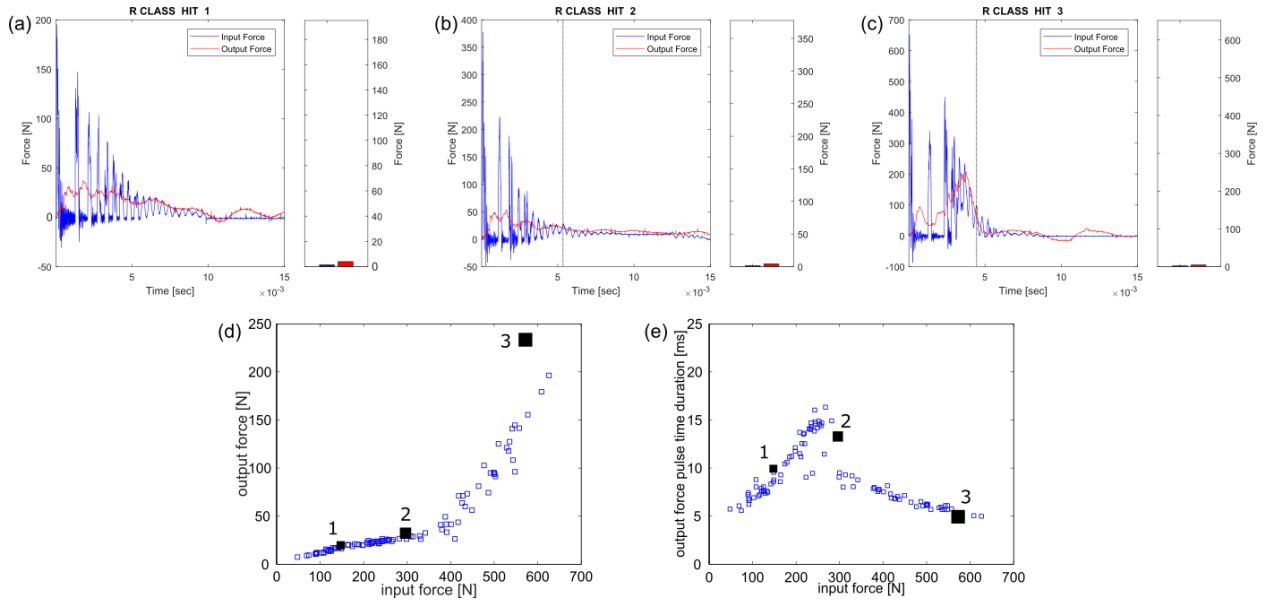

Figure 15: Input and output force time results for each hit of the R-class specimen with corresponding image capture. (a) Hit 1 input versus output force time series (b) Hit 2 input versus output force time series; (c) Hit 3 input versus output force time series; (d) Hit 1-3 position on 100 hit trial results for output versus input force; (e) Hit 1-3 position on 100 hit trial results for output force pulse duration.

The DIC results for the R-class specimen further validate the trends in force transmission established with the Uniform and L-class DIC results. The R-class specimen most closely resembles the force transmission characteristics of the L-class specimen, even though the inner beam is the thickest beam. Just as in the L-class Hit 3, the output force amplitude for Hit 3 presents a small peak interrupted by initial beam buckling, and a much larger peak due to compaction. For the lower amplitude force input hits, there shows a strong initial bimodal response, but, for higher input forces, behavior more aggressively corrects the bimodal response into a collective motion due to the buckling of the thicker middle beam. Upon buckling of this beam, there is a greater snap-through displacement rate which causes higher lateral strain forces than in the bimodal buckling case.

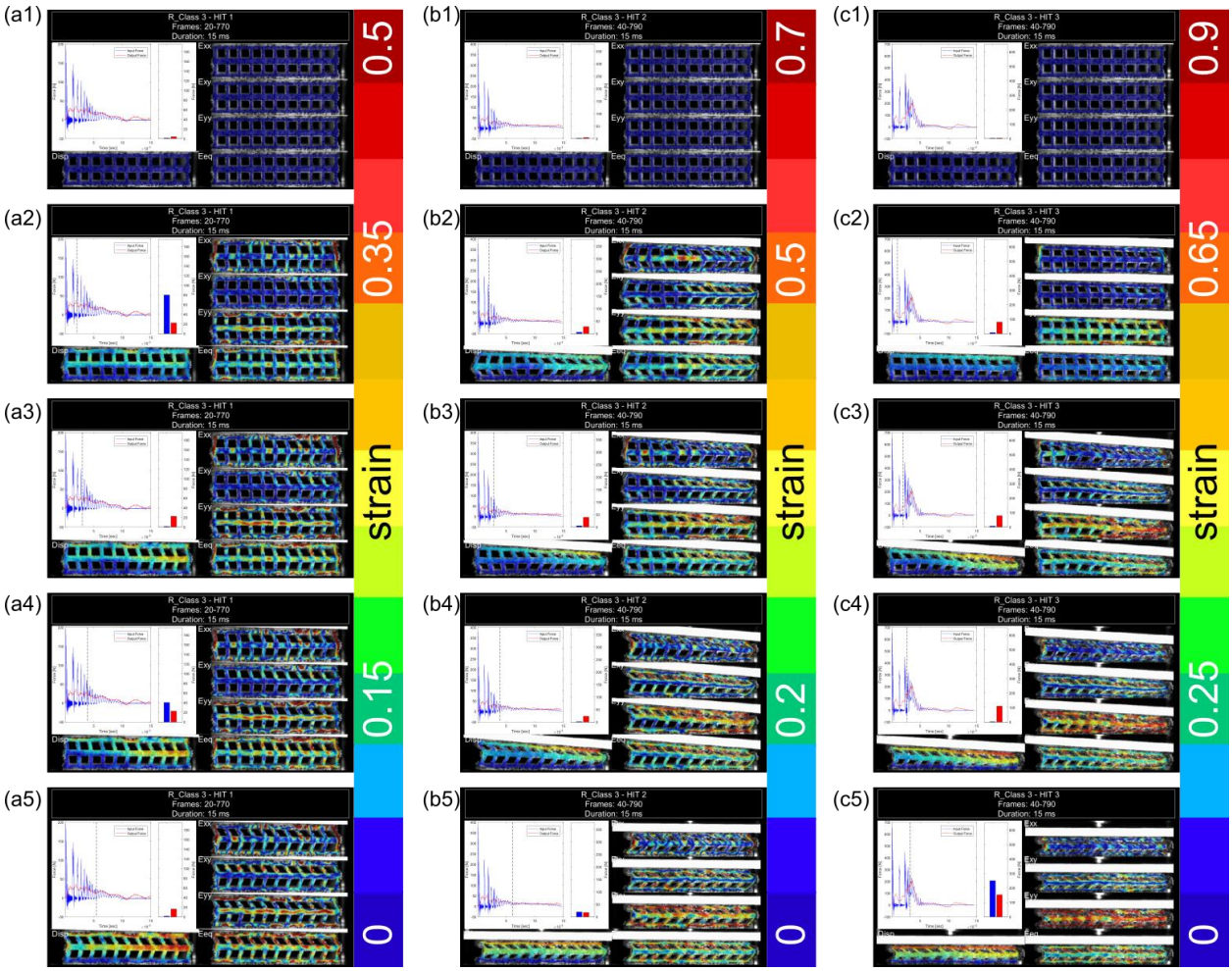

Figure 16: Snapshots highlighting full impact sequence for all three R-class hits: (a) Hit 1, (b) Hit 2, and (c) Hit 3.

4 CONCLUSIONS

Given the importance of attenuating large amplitude impact, it is crucial to understand the dynamic behavior that inevitably occurs impending high amplitude force impact. Specifically, looking at beam-based, elastomeric material systems for their qualities as effective, reusable and lightweight shock absorbers is the focus of this research.

In order to identify and validate the effectiveness of linearly scaled beam variations, termed R- and L- class specimens, as well an array of uniform thick beams, termed Uniform specimens, for varying levels of input force amplitude, it was first necessary to identify the buckling characteristics ultimately being influenced. The L-class specimen buckled uniformly for all levels of force input, whereas the Uniform and R-class specimen initially buckle bimodally but return to uniform collective motion for high impact forces. In addition, the Uniform specimen shows lower force transmission for higher input forces than both the R- and L-class specimens. The Uniform specimen buckles bimodally due to the localization of the impact force above the center of the specimen and the L-class specimen buckles unimodally because the thicker outer beams are more greatly influenced by the translation of the horizontal beam, than by the vertical impact force with regards to direction of buckling.

Future experimentation should consider applying an experimental methodology that applies a uniformly distributed impact across the top of the plates so that all beams are subject to more similar levels of instantaneous loading at the moment of peak input force. This would additionally mitigate results influenced by manual impacting of the plate with a downward swinging motion. It is difficult to rules out the influences of applied shear to the top plate upon impact, given that they are not registered by the modal hammer.

BIBLIOGRAPHY

[1] T. Frenzel, C. Findeisen, M. Kadic, P. Gumbsch and M. Wegener, "Tailored buckling microlattices as reusable light-weight shock absorbers," *Advanced Materials,* vol. 28, no. 28, 2016.

[2] R. L. Harne, J. Bishop, D. Urbanek, Q. Dai and Y. Song, "Extreme impact mitigation by critical point constraints on elastic metamaterials," *The Journal of the Acoustical Society of America,* vol. 141, no. 5, pp. 3643-3643, 2017.

[3] L. Virgin, "The dynamics of symmetric post-buckling," *International Journal of Mechanical Sciences,* vol. 27, no. 7, pp. 235-248, 1985.

[4] B. Florijn and C. a. M. van Hecke, "Programming mechanical metamaterials," *Physical Review Letter,* vol. 113, no. 17, p. 175503, 2014.

[5] L. Wu, X. Xi, B. Li and J. Zhou, "Multi-stable mechanical structural materials," *Advanced Engineering Materials,* vol. 20, no. 2, 2017.

[6] Vicis, Inc., "Vicis," Vicis, 2018. [Online]. Available: https://vicis.com/.

[7] F. Mo, S. Zhao, C. Yu, Z. Xiao and S. Duan, "Design of a conceptual bumper energy absorber coupling pedestrian safety and low-speed impact requirements," *Applied Bionics and Biomechanics,* vol. 2018, no. 9293454, 2018.

[8] R. L. Harne, Y. Song and Q. Dai, "Trapping and attenuating broadband vibroacousic energy with hyperdamping materials," *Extreme Mechanics Letters,* vol. 12, pp. 41-47, 2017.

[9] R. Hetnarski, R. West and J. Torok, "Damping of vibrations of layered elastic-viscoelastic beams," *Applied Mechanics Review,* vol. 46, no. 11S, pp. 305-311, 1993.

[10] S. Cui and R. L. Harne, "Characterizing the nonlinear response of elastomeric material systems," *International Journal of Solids and Structures,* vol. 135, pp. 197-207, 2018.

[11] L. Meza, A. Zelhofer, N. Clarke, A. Mateos, D. Kochmann and J. Greer, "Resilient 3D hierarchical architected metamaterials," *Proceedings of the National Academy of the United States of America,* vol. 112, no. 37, pp. 11502-11507, 2015.

[12] J. Zhou, D. S. L. Liu and Z. Wang, "Application of digital image correlation to measurement of packaging material mechanical properties," *Mathematical Problems in Engineering,* vol. 2013, 2013.

[13] N. McCormick and J. Lord, "Digital Image Correlation," *Materials Today,* vol. 13, no. 12, pp. 52-54, 2010.

[14] P. Vuyk, S. Cui and R. L. Harne, "Illuminating origins of impact energy dissipation in mechanical metamaterials," *Advanced Engineering Materials,* vol. 20, no. 5, p. 1700828, 2017.

[15] S. Shan, S. Kang, J. Raney, P. Wang, L. Fang and F. L. J. B. K. Candido, "Multistable architected materials for trapping elastic strain energy," *Advanced Materials*, pp. 4926-4301, 2015.

5 APPENDIX

5.1 Sample MATLAB code for impact hammer and frame capture experimental data collection

The sample MATLAB code below has the capability to collect a pre-determined total hits for a preset sequence of time intervals (100 hit trials) or on an incoming TTL trigger pulse (image capture for DIC).

```
%% Data acquisition Toolbox NI
clc
clear all

%% Plot styles
colors=['r' 'g' 'b' 'c' 'm' 'k' 'r' 'g' 'b' 'c' 'm' 'k' ];
mtypes=['o' 'v' 's' '^' 'd' 'o' 'v' 's' '^' 'x' 'd'];

%% Acquire data?
global t hitnum
dataacquire=1;  % yes for acquire
DICacquire=1;   % yes if accomanying DIC capture

%% Save data/figs?
% NOTE: dataacquire must also equal one to save
saveon=1; %overwrite is not possible due to timestamp in filename

%% Data acquisition setup parameters
d.fs=131072; % sampling frequency [Hz]. Chosen so that each impact peak has ~4
data points to avoid aliasing
d.filter_data_lo=50; % [Hz] low-pass digital filter frequency
d.filter_data_hi=18000; % [Hz] high-pass digital filter frequency

if DICacquire~=1
    d.seconds=2; % [s] seconds of data acquisition
end

% Create filter
myfilt=designfilt('bandpassiir','filterorder',2,'HalfPowerFrequency1',d.filter
_data_lo,'HalfPowerFrequency2',d.filter_data_hi,'samplerate',d.fs); % filter
result

%% Parameters for hammer impact
d.numhits=3; % target number of(modal hammer impacts) per location
d.threshold_impact_force=40; % [N] any force above this level is flagged as an
impact event
d.time_fft=.15; % [s] time to collect data after each impact
d.target = 150; % Newtons, this parameter is for plotting time series data

if DICacquire~=1
    d.sec_jump=0.01; % TUNABLE PARAMETER [s] seconds to jump forward after
each impact registration. Each impact must occur in less time than this value
end

%% Test specimen name and constraint
d.specimen='R_CLASS_3'; % specimen name, or no_specimen if none
d.constraint_height=0.4600; % [inch] height of constrained/compressed specimen
```

```
%% Filename for d struct
c=clock;

% Use for re-saving plots from pre-existing data
%   d.filename =
'2017_06_08_15_54_25_hammer_lv2_wp79375_dw02_constr_0p46_DIC_impact.mat';

% DEFAULT
constraint = mat2str(d.constraint_height); constraint = constraint(3:end); %
Converts numeric constraint to character type for file naming
if d.numhits <= 3  % Trial is DIC specific
    d.filename=[num2str(c(1)) '_' num2str(c(2),'%02.0f') '_'
num2str(c(3),'%02.0f') '_' num2str(c(4),'%02.0f') '_' num2str(c(5),'%02.0f')
'_' num2str(c(6),'%02.0f') '_hammer_' d.specimen '_constr_0p' constraint
'_DIC_impact.mat'];
else % Trial is taken without DIC images
    d.filename=[num2str(c(1)) '_' num2str(c(2),'%02.0f') '_'
num2str(c(3),'%02.0f') '_' num2str(c(4),'%02.0f') '_' num2str(c(5),'%02.0f')
'_' num2str(c(6),'%02.0f') '_hammer_' d.specimen '_constr_0p' constraint
'_impact.mat'];
end

fige1='_decay_rate_force.fig';
fige2='_amplitude_input_output.fig';
d.figname1=strcat(d.filename(1:end-4),fige1);
d.figname2=strcat(d.filename(1:end-4),fige2);

%% Sensor sensitivity
d.sensor{1}='PCB_086C03_LW39872_force_transducer_impact_hammer';
d.ch_sens(1)=1/0.00235; % N/V
d.sensor{2}='PCB_208C03_LW46472_force transducer_below_specimen';
d.ch_sens(2)=1/0.002232; % N/V
d.nn_chan=length(d.ch_sens);

%% Mean sensor values
% this only plays a role in determining mean-square responses if relevant
d.data_mean(1)=0; % mean force transducer voltage [V]

%% Data Acqusition
if dataacquire==1 % 1=yes for acquire

     % identify connected devices
    devices=daq.getDevices; %once obtained, ensure using correct device name
in below session and acquire lines

    s = daq.createSession('ni');
    ch1 = addAnalogInputChannel(s, 'Dev1', 2, 'Voltage');
    ch2 = addAnalogInputChannel(s, 'Dev1', 3, 'Voltage');

    if DICacquire==1
        hitnum=1;

        ch3 = addAnalogInputChannel(s, 'Dev1', 5, 'Voltage');

        % Set acquisition configuration for each channel
```

```
        ch1.Range = [-10.0 10.0];
        ch2.Range = [-10.0 10.0];
        ch3.Range = [-10.0 10.0];

        % Set acquisition rate, in scans/second
        s.Rate = 131072;

        % Specify the desired parameters for data capture and live plotting.
        % The data capture parameters are grouped in a structure data type,
        % as this makes it simpler to pass them as a function argument.

        % Specify triggered capture timespan, in seconds
        capture.TimeSpan = 0.5;

        % Specify continuous data plot timespan, in seconds
        capture.plotTimeSpan = 0.5;

        % Determine the timespan corresponding to the block of samples
supplied to the DataAvailable event callback function.
        callbackTimeSpan = double(s.NotifyWhenDataAvailableExceeds)/s.Rate;
        % Determine required buffer timespan, seconds
        capture.bufferTimeSpan = max([capture.plotTimeSpan,
capture.TimeSpan*3,callbackTimeSpan * 3]);
        % Determine data buffer size
        capture.bufferSize =  round(capture.bufferTimeSpan * s.Rate);

        % Display graphical user interface
        hGui = createDataCaptureUI(s);

        % Add a listener for DataAvailable events and
        % specify the callback function
        dataListener = addlistener(s, 'DataAvailable', @(src,event)
dataCapture(src, event, capture, hGui,d));

        % Add a listener for acquisition error events which might occur during
background acquisition
        errorListener = addlistener(s, 'ErrorOccurred', @(src,event)
disp(getReport(event.Error)));

        % Start continuous background data acquisition
        s.IsContinuous = true;
        startBackground(s);

        % Wait until session s is stopped from the UI
        while s.IsRunning
            pause(0.5);
        end

        d.data_store=t.data_store(:,:,1:2);
        d.trigsig=squeeze(t.data_store(:,:,3));
        d.time_series=t.time_series;
        d.hitInd=t.hitInd;

        clear t hitnum
```

```
        delete(dataListener);
        delete(errorListener);
        delete(s);
    else
        d.hitInd=zeros([1,d.numhits]);
        pause(2) % pause allows user to move to new location
        iii=1;
        while iii<=d.numhits
            % sound signals user to hit immediately
            asdf=linspace(1/8192,1/4,2048);sound(sin(2*pi*800*asdf),8192)

            % data acquisition
            % prepare to output data on StartForeground
            queueOutputData(s,output_data);
            [d.data,d.time]=s.startForeground; % collect data for one impact
            d.data_store(:,iii,:)=d.data;  % append data to stored matrix
            % append timeseries to stored matrix
            d.time_series(:,iii)=d.time;
            % check if impact occurred with enough data after
            % impact for processing
            hitIndCheck=find(abs(d.ch_sens(1).*d.data(1:end-
d.time_fft*d.fs,1))>d.threshold_impact_force,1,'first');
            if isempty(hitIndCheck)
                % do nothing, repeat this iteration through the loop
            else
                % % if hit did occur, append to stored matrix
                d.hitInd(1,iii)=hitIndCheck;
                iii=iii+1;% if hit did occur, increase counter
            end
            % clear data for next loop
            % d.data=[];
            % d.time=[];
            hitIndCheck=[]; % clear data for next loop
        end
    end

end

%% Take FFT of data
% # of samples to grab from impact time to compute fft
samples_ahead=round(d.fs*d.time_fft);
nft=2^nextpow2(2*samples_ahead);
d.f_ft=d.fs/2*linspace(0,1,nft/2+1)';           % define frequency vector
% make exponential window to scale the impact-induced
% displacement ring-down data
window_hold=exp(-4*[1:samples_ahead]'/d.fs);
%% Process FFT and hit data
d.tf=[];d.tf_meanoutput=[];d.tf_meansq=[];d.tf_mean=[];
data_ft=[];tf_data_on_force=[];data_here=[];

for iii=1:d.numhits
    % filter data
    ch_f=squeeze(filtfilt(myfilt,d.data_store(:,iii,:))); %

    % find the start of the impulse peak (voltage crosses 0)
```

```
    temp_ind_1=find(ch_f(:,1) == max(ch_f(:,1)),1,'first')-300;

    % find the end of the impulse peak (voltage crosses 0)
    temp_ind_2=find(ch_f(:,1)<-0.001,1,'last');

    if DICacquire==1
        % # of samples to grab from impact time to compute fft
        samples_ahead=temp_ind_2-temp_ind_1+1;
        nft=2^nextpow2(2*samples_ahead);
        d.f_ft=d.fs/2*linspace(0,1,nft/2+1)';  % define frequency vector
        window_hold=exp(-4*[1:samples_ahead]'/d.fs);
    end

    % find amplitude of input force
    d.force_amplitude(iii)=max(d.ch_sens(1)*ch_f(:,1));
    % find amplitude of output force
    d.output_amplitude(iii,1)=max(d.ch_sens(2)*ch_f(:,2));

    data_here=d.ch_sens(2).* ...
        ch_f(temp_ind_1:temp_ind_2,1);  % current evaluation of force data

    % compute decay rate of impulse response from exponential fit of
    % amplitude peaks
    atrunc=1:round(.1*length(data_here(:,1)));
    % finding peaks from abs data
    [holding1,holdind1]=findpeaks(abs(data_here(atrunc,1)));
    [holding2,holdind2]=findpeaks(holding1);    % refine peaks
    temptime=[1:length(data_here(atrunc,1))]/d.fs;% create dummy time series
    temp_fit=fit(temptime(holdind1(holdind2))',holding2,'exp1');
    figure(101);clf;box on;
    plot(temptime(holdind1(holdind2))',holding2,'or', ...
        temptime(holdind1(holdind2))',temp_fit.a.* ...
        exp(temp_fit.b*temptime(holdind1(holdind2))'),'-b');
    set(gca,'yscale','log');
    axis([0 .025 1e-2 100]);
    drawnow

    d.decay_rate(1,iii,1)=temp_fit.b;

    % mean of start/stop data in this time frame
    data_mean_here(1)=mean(data_here(:,1));
    % impact fft on disp, take fast fourier transform of exponentially
    % windowed data
    data_ft=fft((data_here-data_mean_here).*window_hold,nft)/ ...
        (samples_ahead*mean(window_hold));

    tf_data_on_force=data_ft(:,1)./d.force_amplitude(iii);
    % impact fft on tf, magnitude of single-sided fourier transform
    disp(nft)
    disp(samples_ahead)
    d.tf(:,iii)=tf_data_on_force(1:nft/4+1);
end

% take mean across hits at location iii
d.tf_mean=mean(d.tf,2);
```

```
% take mean across all locations
d.tf_meansq=mean(d.tf_mean.^2,2);

%% Save data
if saveon==1 && dataacquire==1
    % remove data time series for memory-saving
    d.tf=[];
    d.tf_meanoutput=[];
    d.time=[];
    d.data=[];
%     d.time_series=[];
%     d.data_store=[];

    save(d.filename,'d');
end

%% Plotting time series data
figure(102);
clf;
hold on
box on
% plot time series
plot(d.time_series(:,1),d.data_store(:,1,1)*d.ch_sens(1), ...
     d.time_series(:,1),d.data_store(:,1,2)*d.ch_sens(2));
% plot trigger time if DIC was acquired
if DICacquire==1
    % calculate trigger time
    triggertime =
d.time_series(find(d.trigsig(:,1)==max(d.trigsig(:,1)),1,'first'),1);
    plot([triggertime triggertime],[0 500],'-.');
end

xlabel('Time (s)');
ylabel('Output [N]');
title({[strrep(d.filename,'_','-')] ...
    ['time series, hit: ' num2str(1)] [num2str(d.numlocs) ' input locs with
' ...
    num2str(d.numhits) ' hits each and ' num2str(d.numoutputs) ' output
locs']});

%% Plotting decay rate v force amplitude
colorplot=1;
figure(103);
clf;
hold on
box on
plot(d.force_amplitude,abs(d.decay_rate),[colors(colorplot)
mtypes(colorplot)]);
xlabel('force [N]');  %  xlim([0 450]);
ylabel('decay rate'); %  ylim([0 400]);
title({[strrep(d.filename,'_','-')] ...
       ['decay rate v force'] [num2str(d.numlocs) ' input locs with ' ...
       num2str(d.numhits) ' hits each and ' num2str(d.numoutputs) ...
       ' output locs. height constraint ' num2str(d.constraint_height) '
inch']});
```

```
if saveon == 1
    savefig(d.figname1);
end

% Display force amplitude of hit
fprintf('\ndecay rate:');
display(d.decay_rate(time_series_set));
fprintf('\n');

%% Plotting output amplitude max v force amplitude max
colorplot=1;
figure(104);
clf;
hold on
box on
plot(d.force_amplitude,d.output_amplitude,[colors(colorplot)
mtypes(colorplot)]);
xlabel('input force [N]');   %xlim([0 450]);
ylabel('output force [N]'); % ylim([0 200]);
title({[strrep(d.filename,'_','-')] ...
       ['output amplitude v force'] ...
       [num2str(d.numlocs) ' input locs with ' num2str(d.numhits) ...
       ' hits each and ' num2str(d.numoutputs) ...
       ' output locs. height constraint ' num2str(d.constraint_height) '
inch']});

if saveon == 1
%     savefig(d.figname2);
end

fprintf('\ninput force:');
display(d.force_amplitude(time_series_set))
fprintf(' N\n');
```

5.2 Sample MATAB code for data collection on trigger input

That MATLAB code below is a function required to run the script provided in Section 5.2 if image capture on an input trigger is desired. The function is called as a data listener to create first in first out (FIFO) data buffer that is saved upon a TTL input trigger pulse.

```
function dataCapture(src, event, c, hGui,d)
% Modified from original  MATLAB files exchange script
% Software-Analog Triggered Data Capture
% https://www.mathworks.com/help/daq/examples/software-analog-triggered-data-
capture.html

%dataCapture Processes data for a DIC associated
% impact experiment
global t hitnum
persistent dataBuffer trigActive trigMoment
% If dataCapture is running for the first time, initialize persistent vars
if event.TimeStamps(1)==0
    dataBuffer = [];          % data buffer
    trigActive = false;       % trigger condition flag
```

```
    trigMoment = [];          % data timestamp when trigger condition met
    prevData = [];            % last data point from previous callback
execution
else
    prevData = dataBuffer(end, :);
end
% Store continuous acquisition data in persistent FIFO buffer dataBuffer
latestData = [event.TimeStamps, event.Data];
dataBuffer = [dataBuffer; latestData];
numSamplesToDiscard = size(dataBuffer,1) - c.bufferSize;
if (numSamplesToDiscard > 0)
    dataBuffer(1:numSamplesToDiscard, :) = [];
end
% Update live data plot
% Plot latest plotTimeSpan seconds of data in dataBuffer
samplesToPlot = min([round(c.plotTimeSpan * src.Rate), size(dataBuffer,1)]);
firstPoint = size(dataBuffer, 1) - samplesToPlot + 1;
% Update x-axis limits
xlim(hGui.Axes1, [dataBuffer(firstPoint,1), dataBuffer(end,1)]);
% Live plot has one line for each acquisition channel
for ii = 1:numel(hGui.LivePlot)
    if ii==3
        sens=1;
    else
        sens=d.ch_sens(ii);
    end
    disp(sens)
    set(hGui.LivePlot(ii), 'XData', dataBuffer(firstPoint:end, 1), ...
                           'YData', sens.*dataBuffer(firstPoint:end, 1+ii))
end
% If capture is requested, analyze latest acquired data until a trigger
% condition is met. After enough data is acquired for a complete capture,
% as specified by the capture timespan, extract the capture data from the
% data buffer and save it to a base workspace variable.

% Get capture toggle button value (1 or 0) from UI
captureRequested = get(hGui.CaptureButton, 'value');
if captureRequested && (~trigActive)
    % State: "Looking for trigger event"
    % Update UI status
    set(hGui.StatusText, 'String', 'Waiting for trigger');
    % Get the trigger configuration parameters from UI text inputs and
    %   place them in a structure.
    % For simplicity, validation of user input is not addressed in this
example.
    trigConfig.Channel = sscanf(get(hGui.TrigChannel, 'string'), '%u');
    trigConfig.Level = sscanf(get(hGui.TrigLevel, 'string'), '%f');
    % Determine whether trigger condition is met in the latest acquired data
    % A custom trigger condition is defined in trigDetect user function
    % Condition for signal trigger level
    trigMoment = [];
    if any(latestData(:, 4) > 5)
        % Find time moment when trigger condition has been met
        trigTimeStamps = latestData(trigCondition, 1);
        trigMoment = trigTimeStamps(1);
    end
```

```
elseif captureRequested && trigActive && ((dataBuffer(end,1)-trigMoment) >
c.TimeSpan)
    % State: "Acquired enough data for a complete capture"
    % If triggered and if there is enough data in dataBuffer for triggered
    % capture, then captureData can be obtained from dataBuffer.

    % Find index of sample in dataBuffer with timestamp value trigMoment
    trigSampleIndex = find(dataBuffer(:,1) == trigMoment, 1, 'first')-7000;
    % Find index of sample in dataBuffer to complete the capture
    lastSampleIndex = find(dataBuffer(:,1) == trigMoment, 1, 'first')+5999;
    captureData = dataBuffer(trigSampleIndex:lastSampleIndex, :);
    % Reset trigger flag, to allow for a new triggered data capture
    trigActive = false;
    % Update captured data plot (one line for each acquisition channel)
    for ii = 1:numel(hGui.CapturePlot)
        set(hGui.CapturePlot(ii), 'XData', captureData(:, 1), ...
                                  'YData', captureData(:, 1+ii))
    end
    % Update UI to show that capture has been completed
    set(hGui.CaptureButton, 'Value', 0);
    set(hGui.StatusText, 'String', '');
hitIndCheck=find(abs(d.ch_sens(1).*captureData(:,2))>d.threshold_impact_force,
1,'first');
    if isempty(hitIndCheck)
        % do nothing, repeat this iteration through the loop
    else
        % Use assignin function to save the captured data in a base workspace
variable
        t.data_store(:,hitnum,:)=captureData(:,2:4);
        t.time_series(:,hitnum)=captureData(:,1);
        t.hitInd(1,hitnum)=hitIndCheck;
        hitnum=hitnum+1;% if hit did occur, increase counter
        t.hitnum=hitnum;
    end
elseif captureRequested && trigActive && ((dataBuffer(end,1)-trigMoment) <
c.TimeSpan)
    % State: "Capturing data"
    % Not enough acquired data to cover capture timespan during this callback
execution
    set(hGui.StatusText, 'String', 'Triggered');
elseif ~captureRequested
    % State: "Capture not requested"
    % Capture toggle button is not pressed, set trigger flag and update UI
    trigActive = false;
    set(hGui.StatusText, 'String', '');
end
drawnow;
end
```

5.3 Sample MATLAB code for GUI of incoming signals

The MATLAB code below is function that generates a GUI containing the force and signal time series data in the FIFO data buffer. This GUI provides an interface for the user to debug the experimental setup and activate the data buffer for sensitivity to save on trigger.

```
function hGui = createDataCaptureUI(s)
    % Modified from original  MATLAB files exchange script
    % Software-Analog Triggered Data Capture
    % https://www.mathworks.com/help/daq/examples/software-analog-triggered-
data-capture.html

    %CREATEDATACAPTUREUI Creates a graphical user interface for data
capture.
    %   HGUI = CREATEDATACAPTUREUI(S) returns a structure of graphics
    %   components handles (HGUI) and creates a graphical user interface, by
    %   programmatically creating a figure and adding required graphics
    %   components for visualization of data acquired from a DAQ session (S)
    % Create a figure and configure a callback function (executes on window
close)
    hGui.Fig = figure('Name','Software-analog triggered data capture', ...
        'NumberTitle', 'off', 'Resize', 'off', 'Position', [100 100 750
650]);
    set(hGui.Fig, 'DeleteFcn', {@endDAQ, s});
    uiBackgroundColor = get(hGui.Fig, 'Color');
    % Create the continuous data plot axes with legend
    % (one line per acquisition channel)
    hGui.Axes1 = axes;
    hGui.LivePlot = plot(0, zeros(1, numel(s.Channels)));
    xlabel('Time (s)');
    ylabel('Voltage (V)');
    title('Continuous data');
    legend(get(s.Channels, 'ID'), 'Location', 'northwestoutside')
    set(hGui.Axes1, 'Units', 'Pixels', 'Position',  [207 391 488 196]);
    % Create the captured data plot axes (one line per acquisition channel)
    hGui.Axes2 = axes('Units', 'Pixels', 'Position', [207 99 488 196]);
    hGui.CapturePlot = plot(NaN, NaN(1, numel(s.Channels)));
    xlabel('Time (s)');
    ylabel('Voltage (V)');
    title('Captured data');
    % Create a stop acquisition button and configure a callback function
    hGui.DAQButton = uicontrol('style', 'pushbutton', 'string', 'Stop
DAQ',...
        'units', 'pixels', 'position', [65 394 81 38]);
    set(hGui.DAQButton, 'callback', {@endDAQ, s});
    % Create a data capture button and configure a callback function
    hGui.CaptureButton = uicontrol('style', 'togglebutton', 'string',
'Capture',...
        'units', 'pixels', 'position', [65 99 81 38]);
    set(hGui.CaptureButton, 'callback', {@startCapture, hGui});
    % Create a status text field
    hGui.StatusText = uicontrol('style', 'text', 'string', '',...
        'units', 'pixels', 'position', [67 28 225 24],...
        'HorizontalAlignment', 'left', 'BackgroundColor',
uiBackgroundColor);
    % Create an editable text field for the trigger channel
```

```
    hGui.TrigChannel = uicontrol('style', 'edit', 'string', '3',...
        'units', 'pixels', 'position', [89 258 56 24]);
    % Create an editable text field for the trigger signal level
    hGui.TrigLevel = uicontrol('style', 'edit', 'string', '5.0',...
        'units', 'pixels', 'position', [89 231 56 24]);
    % Create text labels
    hGui.txtTrigParam = uicontrol('Style', 'text', 'String', 'Trigger
parameters', ...
        'Position', [39 290 114 18], 'BackgroundColor', uiBackgroundColor);
    hGui.txtTrigChannel = uicontrol('Style', 'text', 'String',
'Channel', ...
        'Position', [37 261 43 15], 'HorizontalAlignment', 'right', ...
        'BackgroundColor', uiBackgroundColor);
    hGui.txtTrigLevel = uicontrol('Style', 'text', 'String', 'Level
(V)', ...
        'Position', [35 231 48 19], 'HorizontalAlignment', 'right', ...
        'BackgroundColor', uiBackgroundColor);

end

function startCapture(hObject, ~, hGui)
    if get(hObject, 'value')
        % If button is pressed clear data capture plot
        for ii = 1:numel(hGui.CapturePlot)
            set(hGui.CapturePlot(ii), 'XData', NaN, 'YData', NaN);
        end
    end
end

function endDAQ(~, ~, s)
    if isvalid(s)
        if s.IsRunning
            stop(s);
        end
    end
end
```